Acta Crystallographica Section B
Structural Science
ISSN 0108-7681

Transmission electron microscopy and electron diffraction study of the short-range ordering structure of α-$LiFeO_2$

Masanori Mitome,[a]* Shigemi Kohiki,[b] Yusuke Murakawa,[b] Kyoko Hori,[b] Keiji Kurashima[a] and Yoshio Bando[a]

[a]Advanced Materials Laboratory, National Institute for Materials Science, Japan, and [b]Faculty of Engineering, Kyusyu Institute of Technology, Japan

Correspondence e-mail: mitome.masanori@nims.go.jp

Received 22 June 2004
Accepted 21 September 2004

The basic structure of α-$LiFeO_2$, lithium iron oxide, is a cubic NaCl-type structure with a lattice constant of 0.42 nm; some short-range ordering characterized by octahedral clusters exists. The local structure of the short-range ordering was investigated by transmission electron microscopy and electron diffraction. A new short-range ordering structure was found in local areas. The local structure has a cubic lattice with a doubled lattice constant. The occupation factors of cations on Wyckoff sites 4(*a*) and 4(*b*) are different from those on 24(*d*) sites, but the stoichiometric composition in cubic clusters is the same as the macroscopic composition. The number of pairs in which iron cations exist in nearest-neighbor sites and next nearest-neighbor sites is reduced in the structure. This means that a magnetic interaction between the iron cations is reduced by cation ordering even without spin ordering at room temperature.

1. Introduction

It is known that the basic structure of α-$LiFeO_2$ is a cubic NaCl-type structure with the space group $Fm\bar{3}m$, with lithium and iron cations randomly occupying sodium sites. It was, however, reported from a neutron diffraction study (Cox *et al.*, 1963) and an X-ray diffraction study (Brunel & Bergevin, 1969) that diffuse scattering intensity appears in addition to the strong diffraction peaks from the basic structure. The diffuse scattering intensity was also observed in electron diffraction studies (Allpress, 1971; Cowley, 1973).

This scattering intensity has been interpreted as arising from the short-range order of the cations (Brunel *et al.*, 1972; Sauvage & Parthé, 1974; De Ridder *et al.*, 1977). The occupancy probabilities of lithium and iron cations are not completely random, but six corners of a given octahedron in the α-$LiFeO_2$ crystal are occupied by three lithium and three iron cations, according to Pauling's electrostatic valence rule (Pauling, 1929).

On the other hand, $LiFeO_2$ exhibits antiferromagnetic behavior below a critical temperature of 90 K. Electron-spin ordering has been investigated by neutron diffraction and it is reported that electron spins in a given (111) plane at low temperature are ordered ferromagnetically and their direction in successive planes alternates as in MnO (Cox *et al.*, 1963). The magnetic lattice structure has a doubled lattice constant compared with the α phase. Furthermore, an anomaly of magnetization at 40 K has been observed (Anderson *et al.*, 1965; Tabuchi *et al.*, 1998; Kohiki *et al.*, 2004). It is expected that the anomalies are related to cation ordering, but the origin is not clear.

In this study we analyzed the local structure of $LiFeO_2$ powder, which shows an X-ray diffraction pattern of the α phase, by electron diffraction and electron microscopy, and found a new short-range ordered structure with a doubled lattice constant like that of the magnetic lattice.

The theory of the short-range ordered structure in α-$LiFeO_2$ is summarized in the next section. Experimental results are described in §3 and a structure model is discussed in §4. Conclusions are shown in §5.

2. Cation short-range ordered structure in α-$LiFeO_2$

Let us consider a binary system that consists of A and B atoms. The macroscopic atomic fractions of A and B atoms in the system are defined as m_A and m_B, respectively. The occupancy probabilities of an A and a B atom on a jth site are defined as σ_j^A and σ_j^B, respectively. The average values of σ_j^A and σ_j^B are coincident with m_A and m_B. The Flinn operator is defined as deviations from the average values (Flinn, 1956)

$$\bar{\sigma}_j = m_A - \sigma_j^A = \sigma_j^B - m_B. \tag{1}$$

From the definition, the following relations can be derived easily

$$\langle \bar{\sigma}_j \rangle = 0, \tag{2}$$

$$\langle \bar{\sigma}_j^2 \rangle = m_A m_B. \tag{3}$$

The kinematical expression of the scattering amplitude can be expressed as

$$A(\mathbf{g}) = \sum_j \left(f_A \sigma_j^A + f_B \sigma_j^B \right) e^{2\pi i \mathbf{g}\cdot\mathbf{r}_j}, \tag{4}$$

where $\boldsymbol{r}_j$ is a position vector for the jth site, and f_A and f_B are atomic form factors for the A and B atoms. This equation can be rewritten by (1) as

$$A(\mathbf{g}) = A_B(\mathbf{g}) + A_D(\mathbf{g}). \tag{5}$$

Here

$$A_B(\mathbf{g}) = (m_A f_A + m_B f_B) \sum_j e^{2\pi i \mathbf{g}\cdot\mathbf{r}_j}, \tag{6}$$

$$A_D(\mathbf{g}) = (f_A - f_B) \sum_j \bar{\sigma}_j e^{2\pi i \mathbf{g}\cdot\mathbf{r}_j}. \tag{7}$$

$A_B(\mathbf{g})$ is the Bragg diffraction contribution and $A_D(\mathbf{g})$ is the diffuse scattering contribution. When $\mathbf{g}$ is a vector of a Bragg reflection, $A_D(\mathbf{g})$ vanishes because of (2) (De Ridder, Van Tendeloo, Van Dyck *et al.*, 1976).

Considering a polyhedron which consists of S lattice points, we assume that the numbers of A and B atoms in the polyhedron are always $m_A S$ and $m_B S$, which are integers. In the case of α-$LiFeO_2$, the polyhedron is an octahedron ($S = 8$) and $m_A = m_B = 0.5$. This polyhedron is called a cluster by De Ridder, Van Tendeloo & Amelinckx (1976). From this assumption, the summation of the Flinn operator in the cluster is zero

$$\sum_{j=1}^{S} \bar{\sigma}_j = 0. \tag{8}$$

The following relation can be derived by squaring the above equation and averaging over the crystal (De Ridder, Van Tendeloo & Amelinckx 1976).

$$\sum_{j=1}^{S} \langle \bar{\sigma}_j^2 \rangle + \sum_{\substack{i\neq j \\ i,j=1}}^{S} \langle \bar{\sigma}_i \bar{\sigma}_j \rangle = 0. \tag{9}$$

From (3) this equation can be rewritten as

$$1 + \frac{1}{S} \sum_{\substack{i\neq j \\ i,j=1}}^{S} \left(\langle \bar{\sigma}_i \bar{\sigma}_j \rangle / m_A m_B \right) = 0. \tag{10}$$

On the other hand, the Warren–Cowley short-range order parameter is defined as (Cowley, 1950)

$$\alpha_i = 1 - p_i^{AB}/m_B. \tag{11}$$

Here p_i^{AB} is the overall probability for an A atom to have a B atom as an ith neighbor. This parameter has the following relationship with the Finn operator (Clapp & Moss, 1966)

$$\alpha_i = \langle \bar{\sigma}_l \bar{\sigma}_{l+i} \rangle / m_A m_B. \tag{12}$$

Here l is arbitrary and $l + i$ indicates the ith nearest-neighbor position of the lth site.

Substituting (12) into (10) leads to the following equation

$$1 + \sum_{m=1}^{\text{in a polyhedron}} k_m \alpha_m = 0. \tag{13}$$

Here k_m is the number of mth nearest neighbors of an atom in the cluster. For example, (13) becomes the following when the cluster is a tetrahedron.

$$1 + 3\alpha_1 = 0. \tag{14}$$

When the cluster is an octahedron, (13) becomes

$$1 + 4\alpha_1 + \alpha_2 = 0. \tag{15}$$

These equations have already been derived by Brunel *et al.* (1972) and Sauvage & Parthé (1974).

The relationship between the short-range order parameter and the diffuse scattering intensity $I_D(\mathbf{g})$ is expressed as (Clapp & Moss, 1966)

$$\alpha_m = C \int_{V^*} I_D(\mathbf{g}) \exp(2\pi i \mathbf{g}\cdot\mathbf{r}_m) \mathrm{d}\mathbf{g}. \tag{16}$$

Here $\mathbf{r}_m$ is a vector connecting the mth nearest neighbors and $\mathbf{g}$ is a reciprocal vector.

$$\mathbf{g} = h\mathbf{a}^* + k\mathbf{b}^* + l\mathbf{c}^*, \tag{17}$$

where h, k and l are Miller indices. C in (16) is a constant that is normalized by

$$C \int_{V^*} I_D(\mathbf{g}) \mathrm{d}\mathbf{g} = 1. \tag{18}$$

Calculating α_1 and α_2 for the octahedral cluster,

$$\alpha_1 = C \int_{V^*} I_D(\mathbf{g}) \frac{1}{3} \Big(\cos \pi h \cdot \cos \pi k + \cos \pi k \cdot \cos \pi l + \cos \pi l \cdot \cos \pi h \Big) \mathrm{d}\mathbf{g}, \quad (19)$$

$$\alpha_2 = C \int_{V^*} I_D(\mathbf{g}) \frac{1}{3} \Big(\cos 2\pi h + \cos 2\pi k + \cos 2\pi l \Big) \mathrm{d}\mathbf{g}. \quad (20)$$

Substituting these equations into (15),

$$C \int_{V^*} I_D(\mathbf{g}) \frac{2}{3} \Big(\cos \pi h + \cos \pi k + \cos \pi l \Big)^2 \mathrm{d}\mathbf{g} = 0. \quad (21)$$

For equation (21) to be satisfied, the diffuse intensity may have a non-zero value only on the surface described by the following equation in reciprocal space.

$$\cos \pi h + \cos \pi k + \cos \pi l = 0. \quad (22)$$

This surface is schematically drawn in Fig. 1(*a*). Following the same procedure for the cubic cluster, the following equation can be derived and the surface on which the diffuse scattering intensity appears is drawn in Fig. 1(*b*).

$$\cos \pi h \cos \pi k \cos \pi l = 0. \quad (23)$$

3. Experiment and results

$LiFeO_2$ powder was synthesized by the calcination of a mixture of Li_2CO_3 and α-Fe_2O_3 powder at 1173 K for 1 h in air. The molar ratio of the mixture was chosen as Li:Fe = 1.2:1.0 in order to obtain the calcined specimen with the stoichiometric composition $LiFeO_2$.

A powder X-ray diffraction pattern taken by synchrotron radiation at KEK-PF (Tsukuba, Japan) is shown in Fig. 2. All peaks can be attributed to the α phase and the lattice constant is 0.4157 nm, which is coincident with that in the references.

The transmission electron microscope (TEM) used in this study is a JEM-3100FEF with a field-emission-type electron source and 300 kV acceleration voltage (Mitome *et al.*, 2004). The microscope has an energy filter in the column that is useful not only for taking energy-filtered images or electron energy-loss spectra, but also for removing the inelastic scattering contribution from the electron diffraction patterns. Since the diffuse scattering intensity that appears in diffraction patterns of α-$LiFeO_2$ is very weak, the energy filter is important if the diffuse scattering is to be clearly observed, especially when observing thick specimens.

The diffraction patterns were recorded by imaging plates (Amemiya & Miyahara, 1988) that have a high sensitivity and a large dynamic range for electron exposure rather than the usual silver halide photo films. It is difficult to record intense diffraction spots and the weak diffuse scattering intensity simultaneously with the usual silver halide films. Using the imaging plates with an energy-filtering microscope is significant to investigate such weak scattering intensities in diffraction patterns as diffuse scattering.

Electron diffraction patterns taken from the specimen are shown in Fig. 3. Sharp diffraction spots are attributed to the cubic NaCl structure with a lattice constant of 0.42 nm. Any additional diffuse scattering intensities between the sharp spots are seen as they appear in previous studies (Allpress, 1971; Cowley, 1973). Complex patterns of the diffuse scattering are cross sections of the surface drawn in Fig. 1(*a*). It can be interpreted as cation short-range ordering of the octahedral cluster.

TEM images in Fig. 3 show high-resolution structure images. Each black dot indicates an array of iron cations that are arranged as in the cubic NaCl structure. Light elements such as lithium and oxygen cannot be observed in these pictures.

From the same specimen we observed other electron diffraction patterns, as shown in Fig. 4. Sharp diffraction spots can be attributed to the cubic NaCl structure, but the lattice constant is 0.83 nm, *i.e.* twice that of the α phase.

The possible reflection conditions are (hkl) with $h + k$, $k + l$, $h + l = 2n$, ($0kl$) with k, $l = 2n$, (hhl) with $h + l = 2n$, ($00l$) with

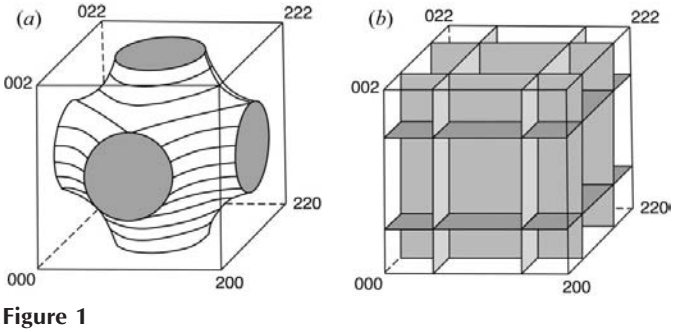

Figure 1
Location of the diffuse scattering intensity in reciprocal space: (*a*) for a case where a cluster, in which the stoichiometric composition is the same as the macroscopic atomic fraction, is an octahedron; (*b*) for a case where the cluster is a cube.

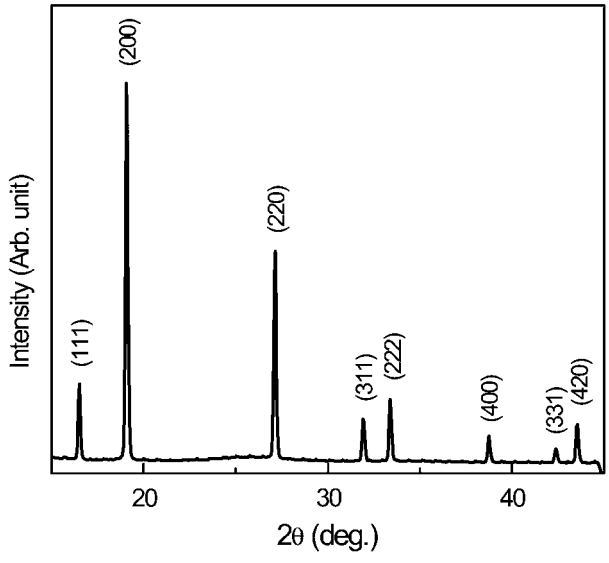

Figure 2
Powder X-ray diffraction spectrum of $LiFeO_2$.

$l = 2n$. The possible space groups are $F23$, $Fm\bar{3}$, $F432$, $F\bar{4}3m$ and $Fm\bar{3}m$.

Some diffuse scattering intensity is also seen in the diffraction patterns in Fig. 4, but it is weaker than that in Fig. 3. Some short-range ordering still exists, but long-range ordering dominates in the doubled-lattice structure.

It is known that the electron-spin ordering structure appears at low temperature and the magnetic lattice constant is doubled (Cox *et al.*, 1963). The spin-ordering structure cannot be detected by electron diffraction because electron spins emitted from the usual electron sources are not polarized. Therefore, the doubled lattice structure observed here results from chemical composition ordering.

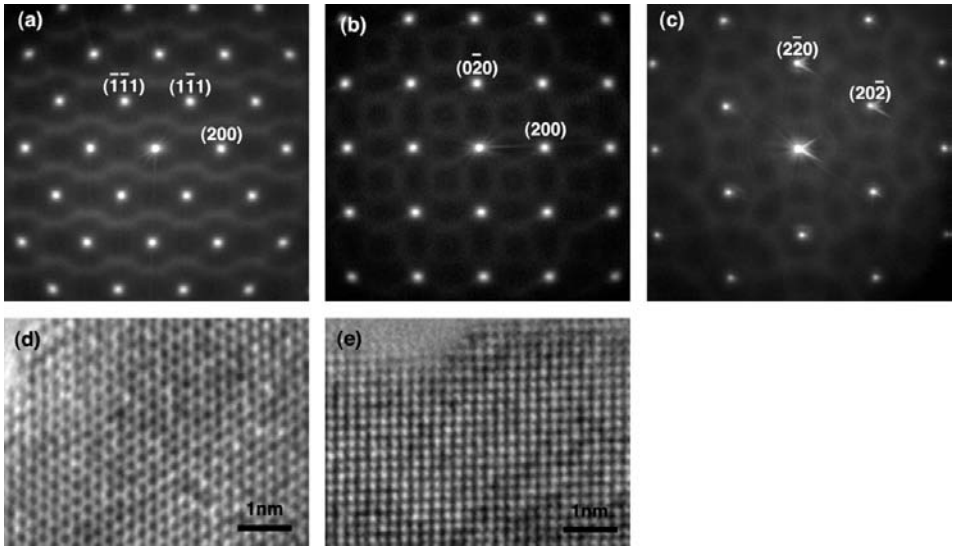

Figure 3
Electron diffraction patterns and TEM images taken from α-$LiFeO_2$. Electron-incident zone axes are (*a*), (*d*) [011], (*b*), (*e*) [001] and (*c*) [111].

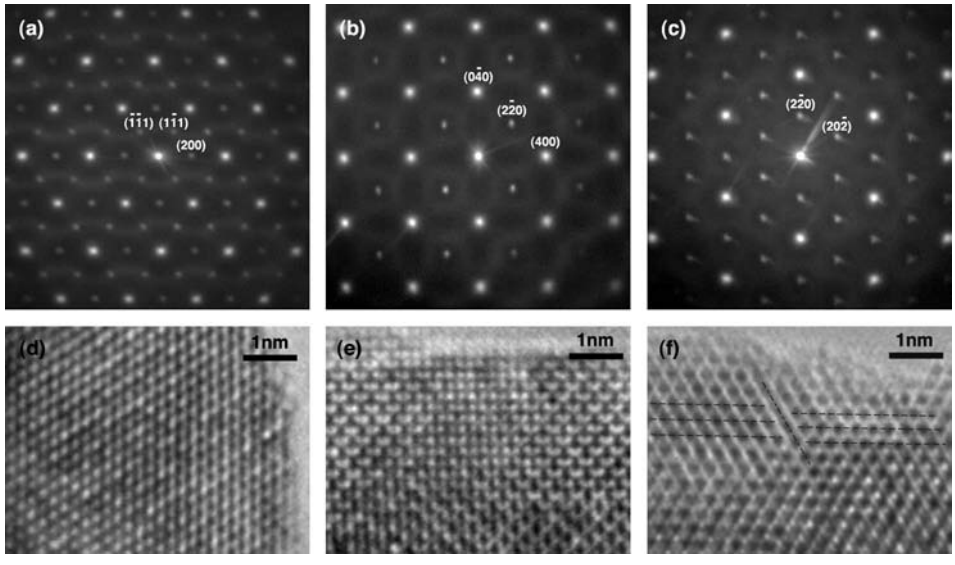

Figure 4
Electron diffraction patterns and TEM images taken from a new short-range ordered structure. Electron incident zone axes are (*a*), (*d*) [011], (*b*), (*e*) [001] and (*c*), (*f*) [111]. A phase boundary is seen in (*f*) (see text).

4. Discussion

The structure model of the doubled-lattice structure is discussed here. It is assumed that the structure has a basic cubic NaCl-type structure and that the cation sites are occupied with lithium and/or iron cations. There are 16 lithium cations, 16 iron cations and 32 oxygen anions included in a unit cell. Hereafter, 32 ion sites that include an origin are called *A* sites and another 32 ion sites are *B* sites. The *A* sites are occupied by cations and the *B* sites by anions, or *vice versa*.

If the space group is $Fm\bar{3}$, $F432$ or $Fm\bar{3}m$, the *A* sites are grouped into three types of equivalent sites by symmetry operations. They are labeled 4(*a*), 4(*b*) and 24(*d*) by multiplicity and Wyckoff letter (see Table 1 and Fig. 5). The *B* sites are grouped into two types of equivalent sites, labeled 8(*c*) and 24(*e*). In the case of $F23$ or $F\bar{4}3m$, the *A* sites are grouped into three types labeled 4(*a*), 4(*b*) and 24(*g*), and the *B* sites are also grouped into three types labeled 4(*c*), 4(*d*) and 24(*f*). The occupancy factors of the equivalent sites must always be the same in order to preserve the symmetry.

If oxygen anions occupy the *A* sites, the 4(*a*) and 4(*b*) sites are equivalent. In this case, the space group becomes $Fm\bar{3}c$ and (111) diffraction is forbidden. This disagrees with the experimental results. It can be assumed without the loss of generality that cations occupy the *A* sites and oxygen anions occupy the *B* sites. In this case, 8(*c*) and 24(*e*) sites in the case of $Fm\bar{3}$, $F432$ or $Fm\bar{3}m$ become equivalent, and 4(*c*), 4(*d*) and 24(*f*) sites in the case of $F23$ or $F\bar{4}3m$ become equivalent. Hereafter it is enough to discuss the case of $Fm\bar{3}$, $F432$ or $Fm\bar{3}m$.

The occupancy factors of the *A* sites are discussed here. The occupancy factors of iron cations on 4(*a*), 4(*b*) and 24(*d*) sites are denoted as $Fe^{(a)}$, $Fe^{(b)}$ and $Fe^{(d)}$. Occupancy factors of lithium cations are denoted as $Li^{(a)}$, $Li^{(b)}$

Table 1
Equivalent sites of a space group.

Sites *A*		Sites *B*	
$Fm\bar{3}$, $F432$ or $Fm\bar{3}m$			
4(*a*)	(000)	8(*c*)	$(\frac{111}{444})$, $(\frac{113}{444})$
4(*b*)	$(\frac{111}{222})$		
24(*d*)	$(0\frac{11}{44})$, $(0\frac{31}{44})$, $(\frac{1}{4}0\frac{1}{4})$, $(\frac{1}{4}0\frac{3}{4})$, $(\frac{11}{44}0)$, $(\frac{31}{44}0)$	24(*e*)	$(t00)$, $(\bar{t}00)$, $(0t0)$, $(0\bar{t}0)$, $(00t)$, $(00\bar{t})$
$F23$ or $F\bar{4}3m$			
4(*a*)	(000)	4(*c*)	$(\frac{111}{444})$
4(*b*)	$(\frac{111}{222})$	4(*d*)	$(\frac{333}{444})$
24(*g*)	$(t'\frac{11}{44})$, $(\bar{t}'\frac{31}{44})$, $(\frac{1}{4}t'\frac{1}{4})$, $(\frac{1}{4}\bar{t}'\frac{3}{4})$, $(\frac{11}{44}t')$, $(\frac{31}{44}\bar{t}')$	24(*f*)	$(t00)$, $(\bar{t}00)$, $(0t0)$, $(0\bar{t}0)$, $(00t)$, $(00\bar{t})$

Lattice coordinates of equivalent sites in space groups. Each coordinate is extended to four coordinates by +(000), $+(0\frac{11}{22})$, $+(\frac{1}{2}0\frac{1}{2})$ and $+(\frac{11}{22}0)$. t and t' are arbitrary values, but they are chosen at $t = \frac{1}{4}$ and $t' = 0$ in this article, because the coordinates show ion sites in an NaCl-type structure.

and $Li^{(d)}$. All sites must be occupied with cations, and thus

$$Fe^{(a)} + Li^{(a)} = 1, \tag{24}$$

$$Fe^{(b)} + Li^{(b)} = 1, \tag{25}$$

$$Fe^{(d)} + Li^{(d)} = 1. \tag{26}$$

The number of iron and lithium cations included in a unit cell is 16 for each.

$$4Fe^{(a)} + 4Fe^{(b)} + 24Fe^{(d)} = 16, \tag{27}$$

$$4Li^{(a)} + 4Li^{(b)} + 24Li^{(d)} = 16. \tag{28}$$

Since (28) can be derived easily from (24)–(27), there are four independent equations with six unknown variables. Two parameters are necessary to express the general solution. The solution is shown in Table 2. Here x denotes $Fe^{(a)}$ and y denotes $Fe^{(b)}$. x and y are within 0–1 and therefore $Fe^{(d)}$ and $Li^{(d)}$ are restricted to between 1/3 and 2/3.

The kinematical structure factors of {002} or {022} reflections are calculated as

$$(16/3)(x + y - 1)(f_{Fe} - f_{Li}). \tag{29}$$

Here f_{Fe} and f_{Li} are the atomic form factors of the Fe and Li atoms. These reflections vanish in the case of $x + y = 1$, even though they are not forbidden by the structure symmetry. Since the {002} and {022} reflections are clearly observed (see Fig. 4), the sum of x and y must be quite different from unity in order to make the {002} and {022} reflections intense enough to be observed.

The kinematical structure factor of {111} reflections is calculated as

$$4(x - y)(f_{Fe} - f_{Li}). \tag{30}$$

This reflection is forbidden when $x = y$. The 4(*a*) and 4(*b*) sites become equivalent in this case. The unit cell is reduced to half the size, which is the same as the α phase, and the space group becomes $Pm\bar{3}m$. This structure model disagrees with the experimental results. The difference between x and y must be large enough to allow the visible intensity of the {111} reflections.

Even though the values of x and y cannot be determined exactly, they may exist in the gray area in x–y space shown in Fig. 6. This means that iron or lithium cations are not distributed on cation sites uniformly, but slightly concentrated on specific sites alternately, for example, on 4(*a*) and 4(*b*) sites. Hereafter, this structure model is called an alternate-distribution model.

Considering the (111) planes, each (111) plane includes 4(*a*) or 4(*b*) sites exclusively. As shown in Fig. 5, the (111) planes including 4(*a*) sites and the (111) planes including 4(*b*) sites are stacked alternately. When iron or lithium cations are concentrated on 4(*a*) sites or 4(*b*) sites, the averaged distance between the same cations becomes larger than if the cations are distributed uniformly as in the α phase.

Each cation site has 12 nearest-neighbor cation sites. The number of nearest-neighbor pairs of cations in a doubled unit

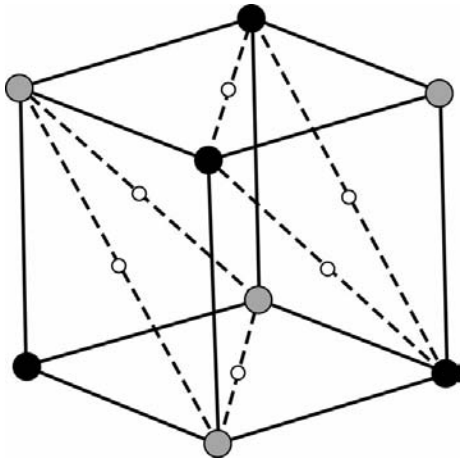

Figure 5
One octant of the doubled unit cell. The black and gray large circles are 4(*a*) and 4(*b*) cation sites, respectively. Open small circles are 24(*d*) cation sites. Oxygen sites are omitted.

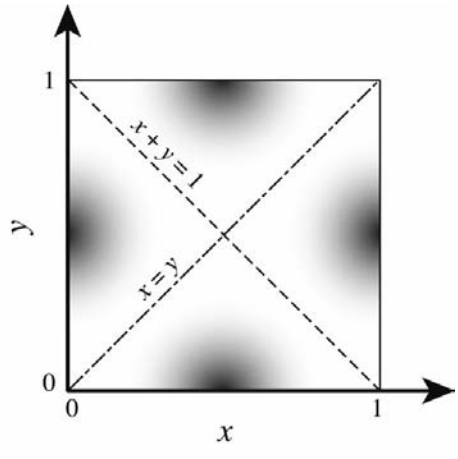

Figure 6
x–y space for the distribution of occupancy factors on 4(*a*) and 4(*b*) sites (see text).

Table 2
Occupancy factors for cation sites.

Wyckoff positions	Fe	Li
4(*a*)	x	$1-x$
4(*b*)	y	$1-y$
24(*d*)	$(4-x-y)/6$	$(2+x+y)/6$

cell is 192, in which 48 pairs of a 4(*a*) site and a 4(*d*) site, 48 pairs of a 4(*b*) site and a 24(*d*) site, and 96 pairs of a 24(*d*) site and a 24(*d*) site are included. The mean number of nearest-neighbor pairs that are occupied by iron cations is expressed as

$$\begin{aligned} B_{nn} &= (1/192)[48x(4-x-y/6)+48y(4-x-y/6) \\ &\quad +96(4-x-y/6)^2] \\ &= -(1/36)(x+y-4)(x+y+2). \end{aligned} \tag{31}$$

The mean number of nearest-neighbor pairs for lithium cations is also expressed as the same equation.

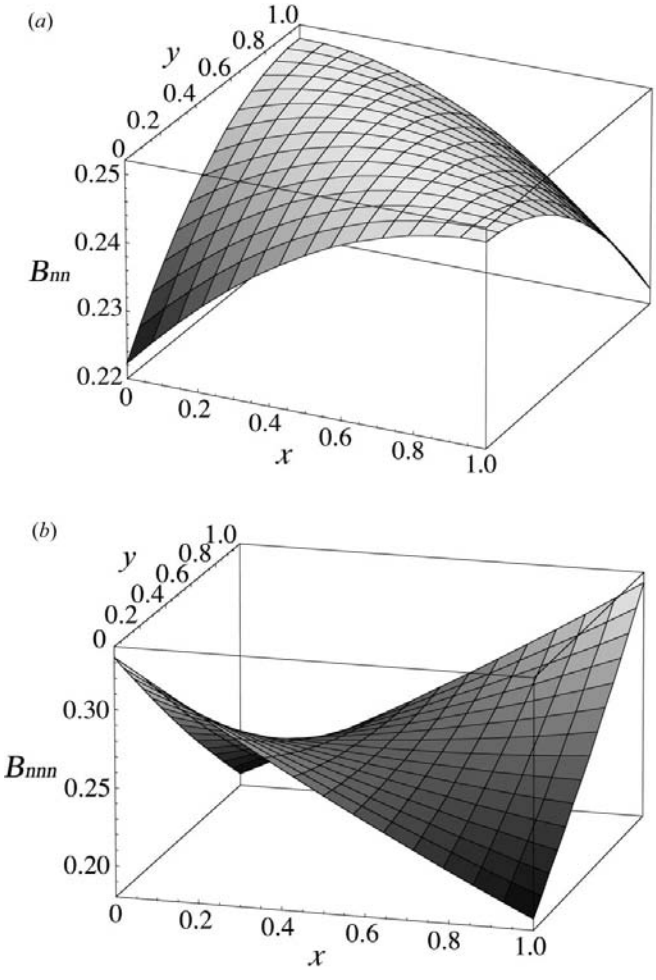

Figure 7
(*a*) The mean number of nearest-neighbor pairs which are occupied by the same cations in a doubled unit cell and (*b*) the number of next nearest neighbor pairs.

When $x + y = 1$, B_{nn} is always 0.25, which is a maximum value. It is also 0.25 for the α phase ($x = y = 0.5$). B_{nn} takes a minimum value of 0.2222 when $x = y = 0$ or $x = y = 1$. The calculated values of B_{nn} are schematically drawn in Fig. 7(*a*).

It is feasible from electron diffraction analysis that the sum of x and y is quite different from unity to obtain {002} and {022} with a diffracted intensity that is strong enough. It corresponds with the fact that B_{nn} becomes small.

Next nearest-neighbor pairs are also important in antiferromagnetic materials because of superexchange interactions. Each cation has six next nearest neighbors *via* the intervening oxygen anions. The next nearest-neighbor sites of a 4(*a*) site are all 4(*b*) sites and vise *versa*. Those of the 24(*d*) sites are all 24(*d*) sites. The mean number of next nearest-neighbor pairs in a unit cell that are occupied by the same cations is

$$\begin{aligned} B_{nnn} &= (1/96)\left[24xy+72(4-x-y/6)^2\right] \\ &= (1/48)\left(x^2+14xy+y^2-8x-8y+16\right), \end{aligned} \tag{32}$$

where B_{nnn} takes a minimum of 0.1875 when $x = 1$, $y = 0$ or $x = 0$, $y = 1$. It takes a maximum of 0.3333 when $x = y = 0$ or $x = y = 1$. It is 0.25 when $x = y = 0.5$; that is the α phase. The calculated values are schematically drawn in Fig. 7(*b*).

The difference between x and y must be large enough to obtain the intense {111} diffracted intensity from (30). It corresponds with the fact that B_{nnn} becomes minimum at $x = 1$, $y = 0$ or $x = 0$, $y = 1$.

Electron-spin ordering occurs at low temperature because of exchange interactions. Six of the 12 nearest-neighbor cations have parallel moments and the other six cations have antiparallel moments. Six next nearest-neighbor cations have antiparallel moments because of the superexchange interaction. The electron spins are however random at room temperature. The number of iron cations which exist at the nearest neighbor sites or the next nearest-neighbor sites of an iron cation decreases in order to reduce the magnetic interactions. To reduce both the nearest neighbors and next nearest neighbors, it is best to set x and y in the gray areas in Fig. 6. It is consistent with the result of the diffraction analysis.

Let us interpret the alternate-distribution model as short-range ordering. Dividing the doubled unit cell into eight cubic sub-cells which have the same size as the α-phase unit cell, each sub-cell includes three 24(*d*) sites, one half a 4(*a*) site and one half a 4(*b*) site (refer to Fig. 5). The number of iron cations included in a sub-cell is

$$\frac{1}{2}\mathrm{Fe}^{(a)}+\frac{1}{2}\mathrm{Fe}^{(b)}+3\mathrm{Fe}^{(d)}=\frac{1}{2}x+\frac{1}{2}y+3(4-x-y/6)=2. \tag{33}$$

The number of lithium cations included in a sub-cell is also two. This means that the stoichiometric composition in each cubic sub-cell is always kept at Li:Fe:O = 1:1:2.

However, the diffraction results cannot be explained by only the cubic cluster model alone. The diffuse scattering intensity appears on a surface drawn in Fig. 1(*b*) when the cluster is a cube. It can be expected that the diffuse scattering

intensity may be observed intensely on half-integral lattice points, for example $(\frac{111}{222})$, $(\frac{113}{222})$, $(\frac{131}{222})$ and so on. These lattice points are expressed as (111) (113) (131) in the doubled unit cell and thus these diffraction spots can be explained by the cubic cluster model.

On the other hand, the forbidden reflections of α-$LiFeO_2$-like (001) and (011) diffraction spots, which are indexed as (002) and (022) in the doubled unit cell, cannot be explained by the cubic cluster model, because the diffuse scattering intensity on these spots vanishes [see (7)]. The alternate-distribution model is necessary to explain all the diffraction results. Therefore, the structure is characterized by both the alternate-distribution model and the cubic cluster.

We must mention the reason why the doubled lattice structure cannot be observed in X-ray diffraction. It is caused by the difference in coherence length. The coherence length of electrons with mutual coherency is estimated by the following equation (Born & Wolf, 1975).

$$0.61(\lambda/\alpha). \qquad (34)$$

Here λ is a wavelength and α is an illumination angle. The wavelength of electrons of 300 keV is 1.97 pm and the illumination angle of the microscope is *ca* 0.1 mrad, and thus the coherence length is 12 nm. On the other hand, the coherence length of X-rays is usually in the μm range and it is much longer than that of an electron.

The doubled lattice structure makes phase boundaries where the lattice unit shifts half (see Fig. 4*f*). The size of the domains surrounded by the phase boundaries is 5 to several 10 nm, which is comparable with the coherent length of the electron but much smaller than that of an X-ray. {002} or {022} reflections diffracted from domains on both sides of a phase boundary interfere and cancel each other. The specimen was observed as the α-phase structure in the X-ray diffraction study. However, electron waves diffracted from neighboring domains do not interfere because the domain size is larger than the coherence length of the electron. Thus, the doubled lattice structure can be revealed by electron diffraction.

5. Summary

The crystal structure of $LiFeO_2$ has been investigated. It is determined as the α phase from X-ray diffraction, but a doubled lattice structure was found in the local structure from electron diffraction. It is a cubic NaCl-type structure like the α phase, but the lattice constant is twice as large.

It is revealed from electron diffraction analysis that the occupancy factors of iron cations are not distributed uniformly, but are concentrated on 4(*a*) or 4(*b*) sites (alternate-distribution model). Simultaneously, the stoichiometric composition in cubic clusters is the same as the macroscopic composition. This structure is characterized by both the alternate-distribution model and the cubic clusters.

The mean number of iron cations that are located at the nearest neighbors or next nearest neighbors of an iron cation is reduced in the doubled lattice structure. This means that magnetic interactions between iron cations are reduced by the chemical ordering even at room temperature, although the spin ordering that appears at low temperature because of exchange interactions does not appear at room temperature.

References

Allpress, J. G. (1971). *J. Mater. Sci.* **6**, 313–318.
Amemiya, Y. & Miyahara, J. (1988). *Nature*, **336**, 89–90.
Anderson, J. C., Dey, S. K. & Halpern, V. (1965). *J. Phys. Chem. Solids*, **26**, 1555–1560.
Born, M. & Wolf, E. (1975). *Principle of Optics*, 5th ed., §10.4, eq. (30). Oxford: Pergamon Press.
Brunel, M. & Bergevin, F. D. (1969). *J. Phys. Chem. Solids*, **30**, 2011–2021.
Brunel, M., Bergevin, F. D. & Gondrand, M. (1972). *J. Phys. Chem. Solids*, **33**, 1927–1941.
Clapp, P. C. & Moss, S. C. (1966). *Phys. Rev.* **142**, 418–427.
Cowley, J. M. (1950). *Phys. Rev.* **77**, 669–675.
Cowley, J. M. (1973). *Acta Cryst.* A**29**, 537–540.
Cox, D. E., Shirane, G., Flinn, P. A., Ruby, S. L. & Takei, W. J. (1963). *Phys. Rev.* **132**, 1547–1553.
De Ridder, R., Van Dyck, D., Van Tendeloo, G. & Amelinckx, S. (1977). *Phys. Status Solidi A*, **40**, 669–683.
De Ridder, R., Van Tendeloo, G., Van Dyck, D. & Amelinckx, S. (1976). *Phys. Status Solidi A*, **38**, 663–674.
De Ridder, R., Van Tendeloo, G. & Amelinckx, S. (1976). *Acta Cryst.* A**32**, 216–224.
Flinn, P. A. (1956). *Phys. Rev.* **104**, 350–356.
Kohiki, S., Murakawa, Y., Kawaguchi, A., Ogawa, K., Hori, K., Shimooka, H., Tajiri, T., Deguchi, H., Mitome, M., Arai, M., Fukushima, S., Bando, Y., Oku, M. & Shishido, T. (2004). *Jpn. J. Appl. Phys.* **43**, L1232–L1235.
Mitome, M., Bando, Y., Golberg, D., Kurashima, K., Okura, Y., Kaneyama, T., Naruse, M. & Honda, Y. (2004). *Microsc. Rec. Tech.* **63**, 140–148.
Pauling, L. (1929). *J. Am. Chem. Soc.* **51**, 1010–1026.
Sauvage, M. & Parthé, E. (1974). *Acta Cryst.* A**30**, 239–246.
Tabuchi, M., Tsutsui, S., Masquelier, C., Kanno, R., Ado, K., Matsubara, I., Nasu, S. & Kageyama, H. (1998). *J. Solid State Chem.* **140**, 159–167.